# First principles calculation of copper-oxide superconductors exhibiting electron fractionalization

Masatoshi IMADA
*Research Institute for Sicence and Engineering, Waseda University,*
*3-4-1 Okubo, Shinjuku-ku, Tokyo, 169-8555*
*Department of Engineering and Applied Sciences, Sophia University.*
*7-1 Kioi-cho, Chiyoda-ku Tokyo, 102-8554*
*and*
*Toyota Physical and Chemical Research Institute,*
*41-1 Yokomichi, Nagakute, Aichi, 480-1192*

## Abstract

We review recent *ab initio* studies on high-$T_c$ superconductivity in copper oxides and insights into basic science of strongly correlated electron systems gained by extensive simulations enabled by supercomputers. After deriving effective Hamiltonians for a number of copper oxide compounds, they were solved by a state-of-the-art quantum many-body solver. The solutions show $d$-wave superconducting states correctly as the ground states. They are severely competing with the charge inhomogeneous states such as spin/charge stripes in accordance with the experimental indications. The amplitude of the superconducting order parameter and its carrier concentration dependence in the ground state well reproduce the experimental trend. The results further show that the diverse materials dependence is well captured. From the understanding of the materials dependence, we successfully extract the principal component that controls the strength of the superconductivity. We will also clarify how the superconductivity can be enhanced in the present mechanism beyond the existing materials. The *ab initio* solution also offers insights into electron fractionalization, which was recently proposed based on photoemission and resonant inelastic X-ray scattering results. The quantum entanglement found in the cuprate superconductors is shown to share a common underlying concept with the quantum spin liquids, which show another type of fractionalization described as an electronic spin splintered into two spinons. A unified understanding of the different two fractionalizations is sketched.

## 1 Introduction

Since the discovery of superconductivity in 1986 in copper oxides with quasi-two-dimensional perovskite structure, more than 35 years have already passed. Although a number of new superconductors were discovered since then, the copper oxides still hold the record of the highest critical temperature at ambient pressure. However, its mechanism has not converged to consensus in the community. Nevertheless, new ideas and concepts from the viewpoint of the basic science have been proposed even now. In this sense, the cuprate superconductors occupy a special position in materials science for decades. Among all, the cuprates show strong electron correlation even at temperatures well above the superconducting transition temperature $T_c$, character-

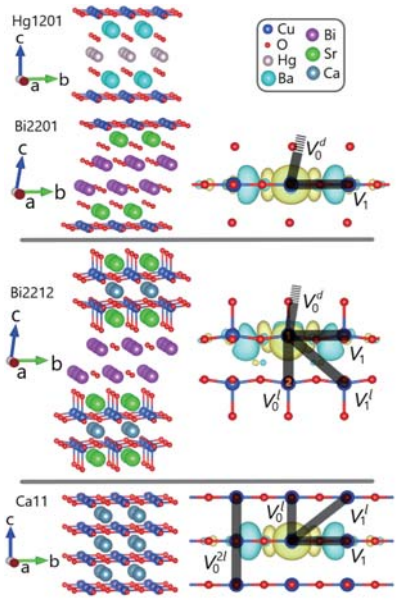


Figure 1: Crystal structure of four cuprate compounds [3]。

ized as the pseudogap in the underdoped region. In addition, the superconducting phase is severely competing with charge inhomogeneous states such as charge striped phases and antiferromagnetic phase. These features invalidate naive mean-field approximations, perturbative treatments from the simple metal and conventional density functional theory, which makes the study difficult. Physical properties including superconductivity itself and its diverse materials dependence of $T_c$ need to be treated from first principles by accurate quantum many-body solvers by taking account of quantum entanglement properly.

Recently, numerical methods to study the strongly correlated electron systems have largely been developed [1], in which effective Hamiltonians derived by an *ab initio* framework starting from given crystal structure without resorting to adjustable parameters have been solved by accurate quantum many-body solvers. We summarize the essence of the results in this report.

In accordance with thus obtained *ab initio* results, electron fractionalization is independently identified as an important origin of the superconductivity and the pseudogap. Namely, it was found that an electron that is an elementary particle in vacuum is emergently splintered in strongly correlated electron systems. Thus generated particles are mutually tunneling quantum mechanically, in other words, hybridizing each other. The fractionalization well accounts for experimental data otherwise puzzling, that was revealed by combining experimental and computational results.

The achievement reviewed in this report would not be reached without the extensive simulations with the aid of supercomputer and the algorithmic progress, where technical details are quite important. However, from the viewpoint of the basic science, the most important achievement is how innovative idea and concept are established as the outcome and how new avenue is opened. In this review, we focus on the understanding of physics achieved in the recent studies by our group. We also address the relation of the electron fractionalization to the electronic spin fractionalization established in *ab initio* as well as model studies of quantum spin liquids.

## 2 *Ab initio* calculations

Numerical method to properly treat the strongly correlated electron systems by deriving effective Hamiltonians describing computationally tractable small degrees of freedom near the Fermi level has been developed for recent two decades [1, 2]. This method is called MACE (multiscale *ab initio* scheme for correlated electrons). Recently MACE has been further improved by using the constrained GW method supplemented by the self-interaction correction [5–7] instead of the conventional constrained random phase approximation (cRPA) [2] to allow better starting point of the global band structure with the proper removal of the double counting of the correlation effect. It is further improved by

introducing the level renormalization feedback (LRFB) to take into account the global self-consistency of the charge density [8].

With these refined procedures, effective Hamiltonians for four families of cuprate superconductors were derived [3], which are carrier doped $CaCuO_2$ (Ca11) (highest suprerconducting transition temperature is $T_c^{\rm opt} \sim 110$K at the optimum carrier doping), $Bi_2Sr_2CuO_6$ abbreviated hereafter as Bi2201 ($T_c^{\rm opt} \sim$ 10-40 K), $Bi_2Sr_2CaCu_2O_8$ abbreviated as Bi2212 ($T_c^{\rm opt} \sim$ 85-100 K), and $HgBa_2CuO_4$ ($T_c^{\rm opt} \sim$ 90K). These four materials share common stacked quasi-two-dimensional $CuO_2$ planes as viewed from the crystal structures in Fig. 1. Although the similar common $CuO_2$ planes are responsible for the superconductivity, the superconducting critical temperatures have diversity as mentioned above. To pursuit the origin of the diversity, conventional density functional theory (DFT) refined by the GW method was applied and global electronic structure was obtained as is shown in Fig. 2. There, a very similar band is crossing the Fermi level $E_F$ (zero energy in Fig. 2), which is identified as the antibonding band (AB band) generated by a strong hybridization of Cu $3d_{x^2-y^2}$ and O $2p_\sigma$ orbitals in the same $CuO_2$ plane. However, other bands away from $E_F$ are largely different.

Since physical properties below room temperatures are determined by the band near the Fermi level in the conventional understanding, the diversity of $T_c^{\rm opt}$ is hardly understood from the similar AB bands. However, the effect of renormalization from the scattered bands may affect the electronic strucure of the AB band due to electron correlation and the original GW band alone is not sufficient to understand the properties below room temperature in the strongly correlated systems. After taking account the effects of the bands away from $E_F$, which renormalizes the AB band, the effective Hamiltonian for the AB band was derived by following the refined MACE procedure [3].

The derived Hamiltonian has the form

$$\mathcal{H} = \sum_{i,j,\sigma} t_{ij} c^\dagger_{i\sigma} c_{j\sigma} + \sum_i U n_{i\uparrow} n_{i\downarrow} + \frac{1}{2} \sum_{i \neq j} V_{ij} n_i n_j, \tag{1}$$

where $i, j$ denotes the Wannier orbital sites of the AB orbital in the $CuO_2$ plane, which are assigned one per Cu atom. By using these site coordinates, $i, j$ dependent hopping $t_{ij}$, onsite interaction, $U$ and interaction $V_{ij}$ between $i$ and $j$ sites are obtained. Here, $c^\dagger_{i\sigma}(c_{i\sigma})$ is the creation (annihilation) operator of the AB orbital electron at $i$ site with the spin $\sigma$.

By taking into account up to the 9th neighbor hopping and interactions in this Hamiltonian without adjustable parameters, the ground states of the 4 families of the cuprate superconductors are obtained [4] by using the many-variable variational Monte Carlo method [9, 10]. Below by considering translational and $C_4$ rotational symmetries of Cu square lattice, we take the notation of $t_1$ to $t_9$ and $V_1$ to $V_9$ in the order of distance for the hopping and interaction, respectively.

In Fig. 3, superconducting pair-pair correlation function $P_d(r)$ is plotted as a function of distance for several choices of $L \times L$ size AB-orbital square lattices and for a number of hole concentrations $\delta$ in the case of hole doped $CaCuO_2$. By using these data, we define $\bar{P}_d(L)$ as $P_d(r)$ converged at long distance for $L \times L$ lattice, which are extrapolated to the thermodynamic limit $L \to \infty$ as one can see in the insets of Fig. 3. Thus obtained $\bar{P}_d^\infty = \lim_{L\to\infty} \bar{P}_d(L)$ show nonzero values indicating $d$-wave superconducting long range order in agreement with the experimental indications.

Hole concentration dependence of the superconducting order parameter $F_{\rm SC}^\infty = \sqrt{\bar{P}_d^\infty}$ obtained from Fig. 3 is shown in Fig. 4, which has the maximum at around $\delta = 0.05$-$0.1$ with a dome structure. It shows monotonic decrease for $\delta > 0.1$, which is consistent with the hole concentration dependence of the superconducting gap observed in the measurement

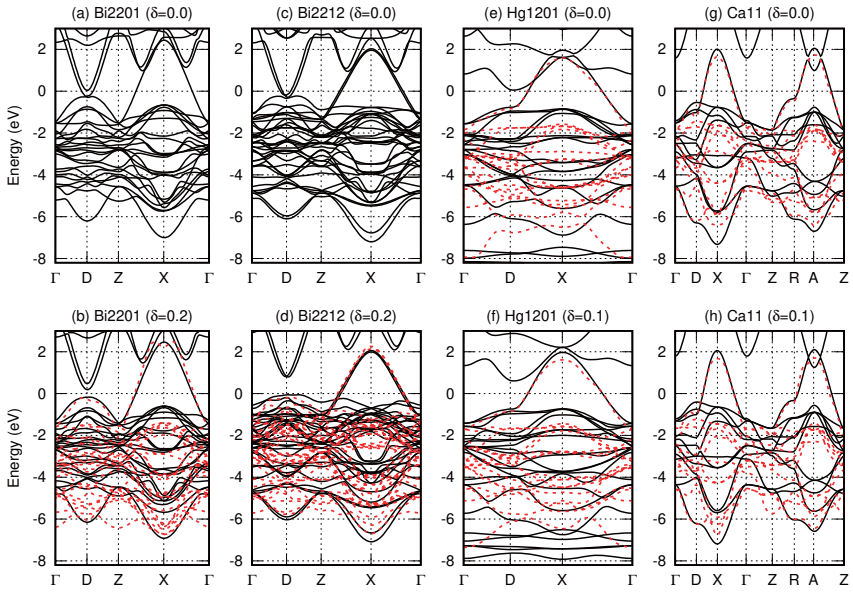


Figure 2: Electronic band structure of 4 cuprate compounds calculated by the GW method [3]. Abscissa represents the wavenumber along the symmetry line and the ordinate is the energy in the unit of eV.

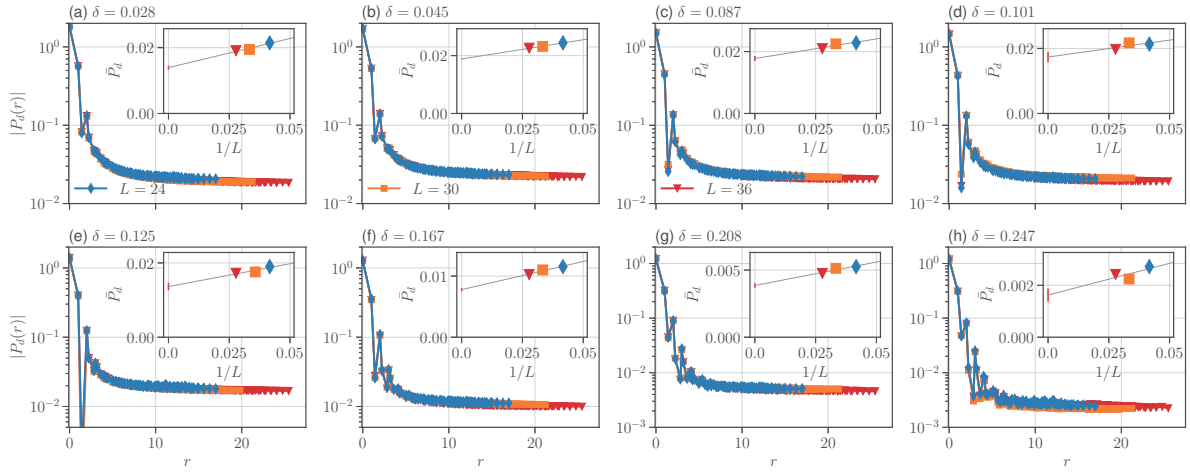


Figure 3: Superconducting correlation of carrier doped $CaCuO_2$ as a function of distance for various system sizes and doping concentrations. Insets show the size extrapolation taken by using the converged value at long distance of each lattice [4].

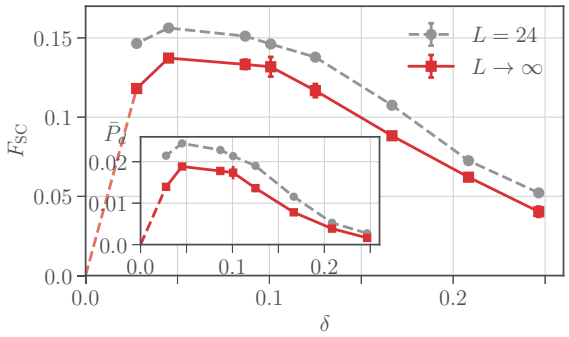


Figure 4: Hole concentration ($\delta$) dependence of superconducting order parameter $F_{\rm SC}^{\infty}$ [4]. Gray symbols are the result of $24 \times 24$ lattice and red symbols are values in the thermodynamic limit [4].

by angle-resolved photoemission spectroscopy (ARPES) and scanning tunneling microscope (STM) [11, 12]. The order parameter at the optimal doping $F_{\rm SC}^{\infty} \sim 0.1$ is also in agreement with the superfluid density determined from the penetration depth measured by the muon spin resonance [13].

On the other hand, this superconducting ground states are severely competing with non-superconducting charge inhomogeneous states with spin-charge stripe orders illustrated in Fig. 5 in the excitation energy scale below 10meV. This also reproduces the widely observed competition in the cuprates.

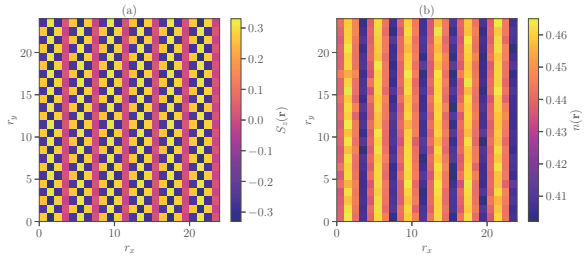


Figure 5: Example of charge and spin density distribution in the real space view of a stripe ordered excited state [4]. (a): Spin density configuration. (b): Chaegr density configuration.

Since the calculated results well reproduce the experimental properties quantitatively, it is now possible to position the status of the cuprate superconductivity in the global perspective, to clarify the superconducting mechanism and to examine the controllability of the superconducting strength all on a realistic ground. In fact, by examining relation between the material dependent diversity of the superconductivity and the parameters of the *ab intio* paramters of the effective Hamiltonians, it was found that the amplitude of the superconducting order parameter $F_{\rm SC}^{\infty}$ is mainly determined by $U/|t_1|$. $U/|t_1|$ is distributed and concentrated between 7 and 9 in the 4 compounds, and they are similar. However, if we plot the relation between $F_{\rm SC}^{\infty}$ and $U/|t_1|$ as one sees in Fig. 6, $F_{\rm SC}^{\infty}$ rapidly and systematically increases with $U/|t_1|$ in the range $7 < U/|t_1| < 8$. Namely if one wants to enhance the superconductivity in most of the realistic compounds, one can do simply by increasing $U/|t_1|$.

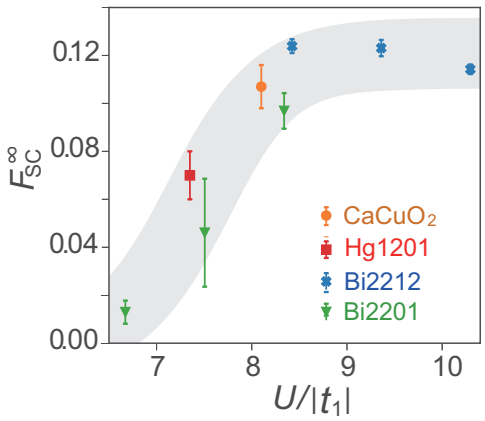


Figure 6: Relation between superconducting order parameter $F_{\rm SC}^{\infty}$ and the *ab initio* parameter $U/|t_1|$ for the 4 family of the cuprates [4].

To understand this trend more clearly, $F_{\rm SC}^{\infty}$ was calculated for the Hamiltonian beyond the *ab initio* parameter values by scaling the onsite $U$ and intersite $V_n$ interactions as $\alpha U$ and $\xi V_n$, respectively as shown in Fig. 7. The scaling of $U/|t_1|$ by $\alpha$ indicates that, if we start from the carrier doped $CaCuO_2$, there exists the maximal enhancement of $F_{\rm SC}^{\infty}$ at slightly larger $U/|t_1|$ than the *ab initio* value, while

it is better to decrease $V_n$ as much as possible and $F_{\rm SC}^{\infty}$ increases to more than twice of the *ab initio* value when $\xi$ vanishes. Within the realistic materials, larger $U/|t_1|$ makes $F_{\rm SC}^{\infty}$ larger. However, if $\alpha$ is increased further, $F_{\rm SC}^{\infty}$ becomes suppressed. In fact, if $U/|t_1|$ is too large, excitonic as well as spin-singlet fluctuations, which generate the quantum entanglement are suppressed and the superconductivity growing from the entanglement are naturally suppressed. Then $\alpha \sim 1.2$ and small $\xi$ beyond the real available material are understood as the optimum condition for the enhancement of superconductivity in the present case. Of course simultaneous tuning toward larger $\alpha$ and smaller $\xi$ is not an easy task in reality, while it provides us with a useful basic guide line for the materials design by the strong-coupling superconducting mechanism.

Now let us come back to the analyses of real materials. It was shown that $T_c^{\rm opt}$ at the optimal doping concentration is well represented by

$$T_c^{\rm opt} \sim 0.16 t_1 F_{\rm SC}^{\infty} \qquad (2)$$

for all the 4 families of the cuprates studied as shown in Fig. 8.

For the Cooper pair formation needed for the superconductivity, effective attractive interaction between electrons is required. To gain insight into the origin of the attraction, carrier concentration ($\delta$) dependence of the energy is plotted in Fig. 9. The total energy of the effective Hamiltonian has of course convex curve with positive curvature for the $\delta$ dependence as is required for the thermodynamic stability for the spatially uniform phase. However, the local energy proportional to $U$ denoted as $E_U$ shows a concave (negative curvature) curve as is shown in Figs. 9 (c) and (d). Therefore, if we expand it with respect to $\delta$ as $E_U = E_0 + a\delta + b\delta^2 + \cdots$, $b$ becomes negative, which immediately means the local attraction because the quadratic coefficient represents the effective carrier interaction. The origin of this emergent local attraction is the following: The

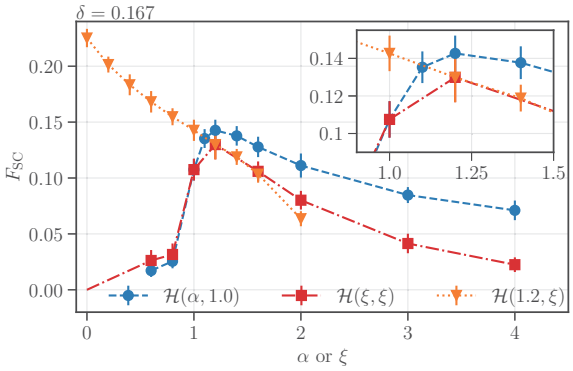


Figure 7: Parameter search of superconducting order parameter $F_{\rm SC}^{\infty}$ in an example starting from *ab initio* parameters of carrier doped $CaCuO_2$ at the hole concentration $\delta = 0.167$. The parameters $U$ and $V_n$ are monitored by scaling $U$ as $\alpha U$, and all the intersite interactions $V_n, n = 1, \cdots 9$ as $\xi V_n$ All the hopping parameters $t_n$ are retained at the *ab initio* values [4]. The case with the monitoring only by $\alpha$ is shown as blue circles, where $F_{\rm SC}^{\infty}$ shows the maximum at $\alpha = 1.2$, with nearly 40 % enhancement from the real hole-doped $CaCuO_2$. On the other hand, if $\alpha$ and $\xi$ are scaled simultaneously, $F_{\rm SC}^{\infty}$ becomes the maximum with 30% enhancement from the *ab initio* value at $\alpha = \xi = 1.2$. The orange upside down triangles show the case by scaling $\xi$ with $\alpha$ fixed at 1.2.

carriers are incoherent and has a large self-energy originally arising from $U$, while the evolution of the carrier doping makes the carriers rapidly coherent (Fermi-liquid like) and the local repulsive interaction energy is reduced nonlinearly causing the negative $b$, which can be regarded as the consequence of the release from the Mottness.

## 3 Electron fractionalization

When the local energy shows such a concave curve, locally bistable energy structure emerges consisting of one stable point in the underdoped side in the left of the concave curve

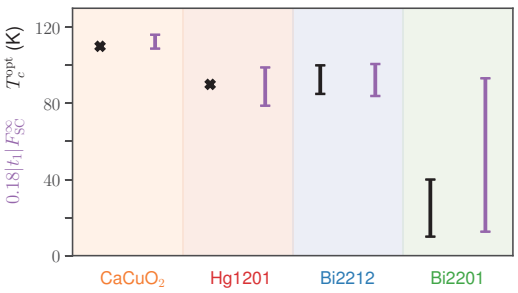


Figure 8: Comparison of experimental $T_c^{\rm opt}$ and the scaling formula $0.16 t_1 F_{\rm SC}^{\infty}$ obtained from the *ab initio* parameter $t_1$ and the calculated order parameter $F_{\rm SC}^{\infty}$. Purple symbols are the prediction by the scaling from the calculation, while the black symbols are the experimental values [4]. For Bi2201 and Bi2212, the error bars are mainly coming from the experimental uncertainty of crystal structure.

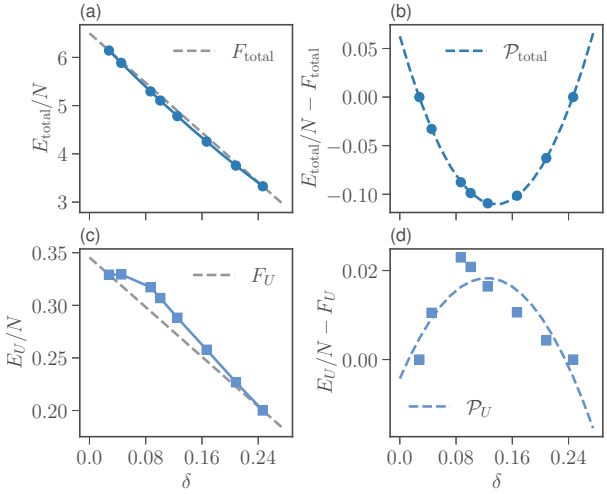


Figure 9: $\delta$ dependence of total energy of the effective Hamiltonian of carrier doped $CaCuO_2$, $E_{\rm tot}$ (a,b) and the energy proportional to $U$ denoted as $E_u$ (c,d) [4]。 In (b,d), $\delta$-linear function $F$ is subtracted for better visibility.

and the other in the overdoped side of the concave curve, which may also be interpreted as the tendency toward the local phase separation. If we introduce the creation (annihilation) of fermion operators to represent the excitation around the two stable region as $c^\dagger, (c)$ for the overdoped region and $d^\dagger, (d)$ for the underdoped region, a simplified two-component fermion model (TCFM) becomes emergently relevant in the following form of a phenomenological Hamiltonian:

$$\begin{aligned} H &= \sum_{k,\sigma}[\epsilon_c(k)c^\dagger_{k,\sigma}c_{k,\sigma} + \epsilon_d(k)d^\dagger_{k,\sigma}d_{k,\sigma} \\ &+ \Lambda(k)(c^\dagger_{k,\sigma}d_{k,\sigma} + \text{H.c.})] \\ &+ \sum_{ij}(v_c(r_{ij})n_{ci}n_{cj} \\ &+ v_d(r_{ij})n_{di}n_{dj} + v_{cd}(r_{ij})n_{ci}n_{dj}). \end{aligned} \tag{3}$$

Here, $\epsilon_c(k)$ and $\epsilon_d(k)$ are the dispersions of $c$ fermion and $d$ fermion, respectively and $\Lambda(k)$ is their hybridization amplitude representing quantum tunneling between these fermions. $v_c$, $v_d$ and $v_{cd}$ are repulsive interactions between two $c$ fermions, between two $d$ fermions and between $c$ and $d$ fermions, respectively. Here, $n_c$ and $n_d$ are the number operators for $c$ and $d$, respectively. If the effects of $v_{cd}$ dominates over $v_c$, $v_d$ and $\Lambda$, segregation of $c$ and $d$ is favored and charge inhomogeneous states such as stripe states in real space become stable. On the contrary, if the effect of $\Lambda$ is dominant, $c$ and $d$ hybridize and make the hybridization gap. This gap is nothing but the pseudogap known in the cuprate superconductors. This Hamiltonian is the simplest one to represent the electron fractionalization into two fermions $c$ and $d$, which is distinct from the earlier proposals of slave boson and slave fermion formalism of fractionalization.

When we introduce the anomalous term $\Delta_c(k)$ and $\Delta_d(k)$ representing the superconducting pairing on the mean-field level, and ignore the interaction between $c$ and $d$ by as-

suming it is small, the TCFM becomes

$$\begin{aligned} H &= \sum_{k,\sigma}[\epsilon_c(k)c^\dagger_{k,\sigma}c_{k,\sigma} + \epsilon_d(k)d^\dagger_{k,\sigma}d_{k,\sigma} \\ &+ \Lambda(k)(c^\dagger_{k,\sigma}d_{k,\sigma} + \text{H.c.}) \\ &+ (\Delta_c(k)c^\dagger_{k,\sigma}c^\dagger_{-k,-\sigma} + \Delta_d(k)d^\dagger_{k,\sigma}d^\dagger_{-k,-\sigma} \\ &+ \text{H.c})], \end{aligned} \tag{4}$$

The Green's function for the $c$ fermion (which can be regarded as the conventional quasiparticle) of the TCFM (4) is given by

$$G_c(k,\omega) = \frac{1}{\omega - \epsilon_c(k) - \Sigma^{\text{nor}}(k,\omega) - W(k,\omega)}. \tag{5}$$

The self-energy contributed from the paired electron and the normal self-energy contributed from the interaction with the normal electrons are

$$W(k,\omega) = \frac{\Sigma^{\text{ano}}(k,\omega)^2}{\omega + \epsilon_c(k) + \Sigma^{\text{nor}}(k,-\omega)^*}, \tag{6}$$

and

$$\Sigma^{\text{nor}}(k,\omega) = \frac{\Lambda(k)^2(\omega + \epsilon_d(k))}{\omega^2 - \epsilon_d(k)^2 - \Delta_d(k)^2}, \tag{7}$$

respectively. Here the anomalous self-energy itself is

$$\Sigma^{\text{ano}}(k,\omega) = \Delta_c(k) + \frac{\Lambda(k)^2\Delta_d(k)}{\omega^2 - \epsilon_d(k)^2 - \Delta_d(k)^2}. \tag{8}$$

In the superconducting state of the TCFM, the normal and anomalous self-energies both have prominent poles (or peaks in the imaginary part) at the same energy $\omega = \pm\sqrt{\epsilon_d(k)^2 + \Delta_d(k)^2}$. However, it was shown that these contributions completely cancel in the total Green' function [14, 15]. Nevertheless, the peak in the anoomalous self-energy is the main origin of the high-$T_c$ superconductivity [14, 16]. Because of the cancellation in the observable Green's function, it has been hidden in the experimental measurements such as ARPES and STM. However, with the help of machie-learning technique, the anomalous and normal contributions were separately extracted from the ARPES data [17] and supported the emergence of the prominet peaks and their cancellations in accordance with the TCFM results [16]. Since the emergence of the peaks accompanied by the cancellation is a unique property of the fractionalized electron, this identification by the machine learning is evidence of the fractionalization.

However, the ARPES data have their own background, noise, and the limitation in the measurable range in the momentum and energy. Therefore, the machine-learning result is not necessarily 100% secured. Therefore, stringent tests by using other independent measurements with different probe are desirable. Recently, the consequence of electron fractionalization on the resonant inelastic X-ray scattering (RIXS) measurement, which can measure the exciton dynamics, was examined. The analysis was made by using TCFM parameters fit by the ARPES data together with the machine learning result. The prediction was that the exciton resonance peak intensity is enhanced in the superconducting phase in comparison to the normal pseudogap phase as one can see in Fig. 10, if the fractionalization is at work [18]. The origin of this enhancement is the increase of the occupied $c$ component below the fermi level in the superconducting phase, because only the $c$ component decays to the core electron and forms an exciton. This prediction was tested experimentally at the NSRRC facility in Taiwan and as in Fig. 11 the exciton peak enhancement in the order of 10% was detected at the optimum doping, where the fractionalization is expected and the normal phase has the pseudogap, in agreement with the prediction, while the enhancement was not observed in the overdoped sample where the fractionalization is not expected [19]. This result further establishes the existence of the electron fractionalization.

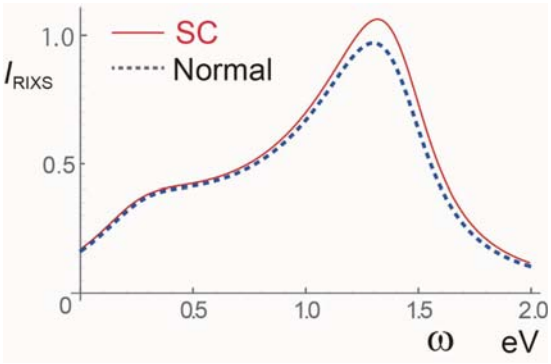


Figure 10: Prediction of the exciton resonance peak in the superconducting phase (red curve) as compared to that in the normal phase (dashed curve) in the presence of the electron fractionalization. The peak is enhanced in the superconducting phase only when the fractionalization is at work [19].

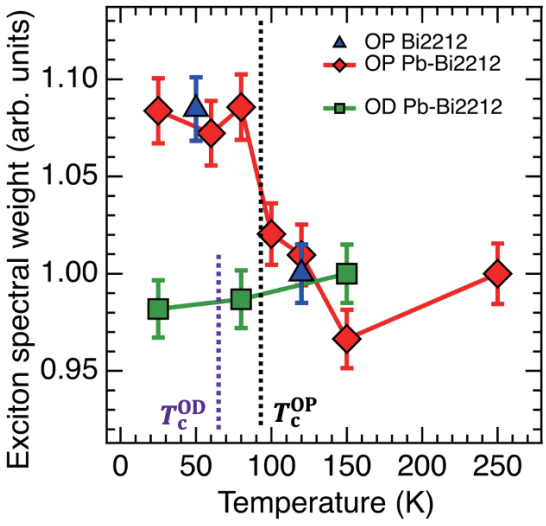


Figure 11: Temperature dependence of the exciton resonance peak measured by RIIXS. The peak is enhanced below $T_c$ only for the sample at the optimum doping (red diamond and blue triangle symbols), where the fractionalization is expected. The intensity does not change in the overdoped sample (green squares), where the fractionalization is not expected [19].

# 4 Summary and outlook – toward unified understanding of fractionalization for high $T_c$ superconductivity and quantum spin liquid

Another challenge of condensed matter physics is the nature of quantum fluids, especially, the quantum spin liquid since the first proposal half a century ago [24]. It was already shown with the aid of supercomputers that the quantum spin liquid phase indeed exists and the spin excitations are well described by the fractionalized spinions in gapless quantum spin liquids, where the spinon has the Dirac-type gapless excitation and an observable spin excitation is represented by the two composite excitations of the spinon [20,21]. *Ab initio* calculations of molecular solid called dmit salts indeed demonstrated that this picture holds [20]. The existence of the quantum spin liquid was also established in a theoretical touchstone model, $J_1$-$J_2$ Heisenberg Hamiltonian on the square lattice, where essentially the same structure of the fractionalized excitation is obtained [21]. These findings were made it possible by the progress in quantum many-body solver using the neural network [25].

The electron fractionalization found in the cuprate superconductors and the fractionalization of an electronic spin into two spinons in the quantum spin liquid look quite different at a glance. However, the essence of the superconducting state as well as the quantum spin liquid lies in the way of constructing quantum mechanically entangled state, the element of which is commonly the paired state of two electrons with further entanglement of the pairs. Figure 12 illustrate a state consisting of the two sites and two electrons with one up and one down electrons, represented by a linear combination of the 4 states, which expand the full Hilbert space composed of the 4 states, with the weight of $a_1$, $a_2$ $a_3$, and $a_4$. If $a_3 = a_4 = 0$

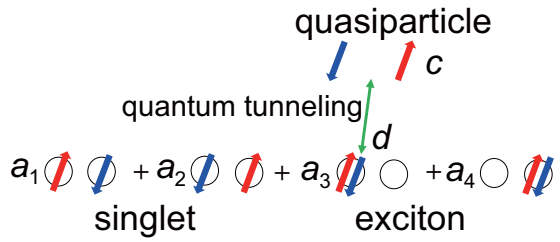


Figure 12: Illustration of the full Hilbert space as a simplified but comprehensive view containing the electron fractionalization in the strong coupling superconductor and the quantum spin liquid in the Mott insulator for two electrons on two sites.

holds in the Mott insulator, the ground state satisfies $a_1 = -a_2$ through the superexchange interaction, which generates the quantum entanglement of the singlet as a component of the quantum spin liquid. On the other hand, if $a_1 = a_2 = 0$ is satisfied, the component with $a_3$ and $a_4$ represents the quantum entanglement of an exciton and a dark fermion $d$ as a fermionic component of the exciton emerges due to the Mottness, where $d$ drives the high-$T_c$ superconductivity. In this sense, the quantum spin liquid and high-$T_c$ Cooper pair are connected as the different component of the originally same entanglement. In Fig. 12, the quasiparticle ($c$ fermion) is spatially extended, which appears when the electron is released from the 4 bound states and is distinct from the dark fermion $d$, while they transform each other by the hybridization, meaning $c$ and $d$ have finite lifetime. In this way, the quantum entanglement by the spin singlet constituting the quantum spin liquid and by the exciton leading to the electron fractionalization are represented in the extended Hilbert space in a unified fashion and the singlet and exciton take on different aspect of the same entanglement.

*Ab initio* calculations of strongly correlated electron systems needed for quantitative understanding and predictive power had faced with large difficulty for decades. In particular, high-$T_c$ superconductivity and quantum mechanically entangled spin liquid had been major challenging targets. However, MACE scheme has one after another suceeded in reproducing first the superconducting properties of strong coupling superconductors such as the iron-based superconductors [22] and the cuprate superconductors [3, 4, 23]. MACE has also succeeded in reproducing the quantum spin liquid in an *ab initio* fashion [20]. The *ab initio* calculations are crucially important in the sense that the understanding of the universal mechanisms that produces the high-$T_c$ superconductivity and the quantum spin liquids as well as materials design become possible only by understanding material dependence quantitatively based only on the crystal structure. On the other hand, the *ab initio* results obtained after solving by sophisticated quantum many-body solvers are, in a sense, black box outcome and its nature is sometimes not intuitively easily understandable. Therefore, to reveal the underlying physics hidden in the calculated results, simplified phenomenological models which capture the essence are quite useful and also help comparisons with experiments.

Next subject to understand electron fractionalization is to derive phenomenological two-component fermion model microscopically from *ab initio* Hamiltonians. On the other hand, determination of the parameters of TCFM are now being made possible from the fitting to the experimental spectroscopic data [15, 18]. To enhance the accuracy of quantitative estimates and predictability, combined analyses of different spectroscopic tools such as the combination of ARPES, RIXS and quasiparticle interference (QPI) derived from STM data have already started. Integrated spectroscopy combined with the *ab initio* calculations and the machine learning aided by supercomputer facility is the future avenue to be pursuied to attack difficult strongly correlated electron systems.

### Acknowledgements

This activity report is based on the collaborations with Michael Schmid, Jean-Baptiste Moree, Youhei Yamaji, Motoaki Hirayama, Yusuke Nomura, Di-Jing Huang, Atsushi Fujimori, Teppei Yoshida, Kota Ido, Takahiro Misawa, and Kazuyoshi Yoshimi. To perform the numerical simulation, computer resources of "Fugaku" (hp190145, hp200132, hp210163, hp220166) under the MEXT project JPMXP1020200104 were utilized. We also thank the facility supported by Supercomputer Center, Institute for Solid State Physics, University of Tokyo. We are also grateful to the financial support of JSPS Kakenhi Grant No. 16H06345, No. 22A202 ("Foundation of Machine Learning Physics ") and No, 22H05114 ("Frontiers of Condensed Matter Physics Pioneered by Neural Network").

## References

[1] M. Imada, and T. Miyake: J. Phys. Soc. Jpn. **79** (2010) 112001.

[2] F. Aryasetiawan, M. Imada, A. Georges, G. Kotliar, S. Biermann, and A.I. Lichtenstein: Phys. Rev. B **70** (2004) 195104.

[3] J.-B. Morèe, M. Hirayama, M. T. Schmid, Y. Yamaji, and M. Imada: Phys. Rev. B **106**, (2022) 235150.

[4] M. T. Schmid, J.-B. Morèe, Y. Yamaji, and M. Imada: unpublished.

[5] M. Hirayama, T. Miyake and M. Imada: Phys. Rev. B **87** (2013) 195144.

[6] M. Hirayama, T. Miyake, M. Imada, and S. Biermann: Phys. Rev. B. **96** (2017) 075102.

[7] M. Hirayama, Y. Yamaji, T. Misawa, and M. Imada: Phys. Rev. B **98** (2018) 134501.

[8] M. Hirayama, T. Misawa, T. Ohgoe, Y. Yamaji, M. Imada: Phys. Rev. B **99** (2019) 245155.

[9] D. Tahara and M. Imada: J. Phys. Soc. Jpn. **77** (2008) 114701.

[10] T. Misawa, S. Morita, K. Yoshimi, M. Kawamura, Y. Motoyama, K. Ido, T. Ohgoe, M. Imada, T. Kato: Comput. Phys. Commun. **235**, (2019) 447.

[11] K. Tanaka, W. S. Lee, D. H. Lu, A. Fujimor, T. Fujii, Risdiana, I. Terasaki, D. J. Scalapino, T. P. Devereaux, Z. Hussain, and Z.-X. Shen: Science **314**, (2006) 1910.

[12] J. Alldredge, J. Lee, K. McElroy, M. Wang, K. Fujita, Y. Kohsaka, C. Taylor, H. Eisaki, S. Uchida, P. Hirschfeld, and J. Davis: Nat. Phys. **4**, (2008) 319.

[13] Y. J. Uemura, G. M. Luke, B. J. Sternlieb, J. H. Brewer, J. F. Carolan, W. N. Hardy, R. Kadono, J. R. Kempton, R. F. Kiefl, S. R. Kreitzman, P. Mulhern, T. M. Riseman, D. L. Williams, B. X. Yang, S. Uchida, H. Takagi, J. Gopalakrishnan, A. W. Sleight, M. A. Subramanian, C. L. Chien, M. Z. Cieplak, G. Xiao, V. Y. Lee, B. W. Statt, C. E. Stronach, W. J. Kossler, and X. H. Yu, Phys. Rev. Lett. **62**, (1989) 2317.

[14] S. Sakai, M. Civelli, and M. Imada: Phys. Rev. Lett. 116 (2016) 057003; Phys. Rev. B. **94** (2016) 115130.

[15] M. Imada: J. Phys. Soc. Jpn. **90** (2021) 111009.

[16] Y. Yamaji, T. Yoshida, A. Fujimori, M. Imada: Phys. Rev. Research **3** (2021) 043099.

[17] T. Kondo, Y. Hamaya, A. D. Palczewski, T. Takeuchi, J. Wen, Z. Xu, G. Gu, J. Schmalian, and A. Kaminski, Nat. Phys. **7** (2011) 21.

[18] M. Imada: J. Phys. Soc. Jpn. **90** (2021) 074702.

[19] A. Singh, H. Y. Huang, J. D. Xie, J. Okamoto, C. T. Chen, T. Watanabe, A. Fujimori, M. Imada, D. J. Huang: Nat. Commun. **13** (2022) 7906.

[20] K. Ido, K. Yoshimi, T. Misawa, and M. Imada: npj Quantum Mater. **7** (2022) 48.

[21] Y. Nomura and M. Imada: Phys. Rev. X **11** (2021) 031034.

[22] T. Misawa and M. Imada: Nat. Commun. **5** (2014) 5738.

[23] T. Ohgoe, M. Hirayama, T. Misawa, K. Ido, Y. Yamaji, M. Imada Phys. Rev. B **101**, 045124 (2020).

[24] P. Fazekas and P. W. Anderson: Phil. Mag. **30** (1974) 423.

[25] Y. Nomura, A. S. Darmawan, Y. Yamaji and M. Imada: Phys. Rev. B **96** (2017) 205152.